Biomedical Engineering Faculty Research and Publications

Biomedical Engineering, Department of

Quantification of Bronchial Circulation Perfusion in Rats

Christian Wieholt
University of Chicago

Robert C. Molthen
Marquette University, robert.molthen@marquette.edu

Steven Thomas Haworth
Medical College of Wisconsin

David L. Roerig
Medical College of Wisconsin

Christopher A. Dawson
Medical College of Wisconsin

See next page for additional authors

Authors

Christian Wieholt, Robert C. Molthen, Steven Thomas Haworth, David L. Roerig, Christopher A. Dawson, and Anne V. Clough

Quantification of Bronchial Circulation
Perfusion in Rats

Christian Wietholt[a], Robert C. Molthen[a,b,c], Steven T. Haworth[b,c],
David L. Roerig[b,c], Christopher A. Dawson[a,b,c]
and Anne V. Clough[a,c]

[a]Marquette University, Milwaukee, WI
[b]Medical College of Wisconsin, Milwaukee, WI
[c]Research Service, Zablocki Veterans Affairs Medical Center, Milwaukee, WI

ABSTRACT

The bronchial circulation is thought to be the primary blood supply for pulmonary carcinomas. Thus, we have developed a method for imaging and quantifying changes in perfusion in the rat lung due to development of the bronchial circulation. A dual-modality micro-CT/SPECT system was used to detect change in perfusion in two groups of rats: controls and those with a surgically occluded left pulmonary artery. Both groups were imaged following injections on separate days i) 2mCi of Tc99m labeled macroaggregated albumin (MAA) into the left carotid artery (IA) and ii) a similar injection into the femoral vein (IV). The IA injection resulted in Tc99m accumulation in capillaries of the systemic circulation including the bronchial circulation, whereas the IV resulted in Tc99m accumulation in the pulmonary capillaries. Ordered subset expectation maximization (OSEM) was used to reconstruct the SPECT image volumes and a Feldkamp algorithm was used to reconstruct the micro-CT image volumes. The micro-CT and SPECT volumes were registered, the SPECT image volume was segmented using the right and left lung boundaries defined from the micro-CT volume, and the ratio of IA radioactivity accumulation in the left lung to IV radioactivity accumulation in both lungs was used as a measure of left lung flow via the bronchial circulation. This ratio was ~0.02 for the untreated rats compared to the treated animals that had an increased flow ratio of ~0.21 40 days after left pulmonary artery occlusion. This increase in flow to the occluded left lung via the bronchial circulation suggests this will be a useful model for further investigating antiangiogenic treatments.

Keywords: small animal, SPECT, micro-CT, lung perfusion imaging, dual-modality imaging, bronchial circulation, angiogenesis, rat

1. INTRODUCTION

Angiogenesis within the lung is thought to be stimulated by carcinoma, providing a blood supply for the increased metabolism of malignant tumors.[1-3] The ability to regulate the blood supply to these tumors is the goal of studies on antiangiogenic drugs currently in development.[4,5] Although generally the bronchial circulation is thought to provide nourishment to the airway walls[6] it has also been shown to play an important role in this angiogenesis.[7] A model of this angiogenesis in the lung is occlusion of one of the pulmonary arteries which has been shown to induce vessel growth in the bronchial circulation of the occluded lung lobe in rats,[8,9] mice[10] and dogs[11] in an attempt to compensate for the lost perfusion via the pulmonary circulation.

Medical imaging[12] is a minimally invasive way of monitoring the structure/function relationship of vessel growth and organ perfusion. Vessels can be visualized using micro-CT and perfusion monitored with SPECT.[13,14] In particular, small animal imaging, utilizing MRI,[15] or functional CT,[16] provides an opportunity to examine new vessel development in animals that have received treatment to promote angiogenesis. A dual-modality

micro-CT/SPECT system provides the opportunity to observe functional changes and locate these changes within the anatomy of the animal. Thus, we have developed a dual-modality micro-CT/SPECT system[17] to monitor angiogenesis in rats with a surgically occluded left pulmonary artery to determine the time course of angiogenesis within the bronchial circulation.

2. PHANTOM STUDY

2.1. Imaging System

The dual-modality imaging system consisted of a Picker DYNA ^{TM} MO gamma camera and a custom-made micro-CT system. The gamma camera had a 260mm diameter sodium iodide scintillation crystal and is equipped with a 5mm pinhole collimator. Data acquisition and digitization of camera output was done by a Siemens MicroDELTA system connected over a high speed bus to a Digital MicroVAX 3300. The camera was positioned in front of the specimen which was mounted on a rotary stage (New England Affiliated Technologies) at a distance of ~60mm (pinhole-to-object) which provided 3× magnification. The micro-CT system consisted of a Feinfocus FXE/FXT 100.20 microfocal x-ray source (with a 3μm focal spot) and an image-intensifier (Thomson TH9438 HX H661 VR24) optically coupled to a CCD camera (Silicon Mountain Design SMD1M-15) as described previously.[18-20] This equipment was mounted on a precision rail with a source-to-object distance of 350mm and a source-to-detector distance of 800mm.

2.2. Imaging Methods

A calibration study was performed with a test phantom that consisted of three test tubes (two 14mm in diameter and one 9mm in diameter) fixed within a 45mm diameter cylinder. Each tube was filled with equal concentrations of Tc99m labeled macroaggregated albumin (MAA) with a total activity of 2mCi. The phantom was placed within a plastic tube (diam=70mm) and positioned on the specimen stage The center of the pinhole was positioned at the same height as the x-ray focal spot. The center of rotation was set so that the whole phantom was within the field of view at all angular positions. A set of 128 projection images was acquired with an acquisition time of 20sec/view. The phantom was then imaged without relocation using the micro-CT system at 360 angular views, with an acquisition time of 233ms/view.

2.3. Image Processing

The image processing, SPECT and micro-CT reconstruction, and the image registration of the dual-modality data was performed on a IBM compatible PC with an AMD Athlon XP 1900+ processor, 1GB of random access memory and a GeForce 4 Ti4600 graphics card for 3D visualization. The operating system was Red Hat Linux 7.3 with a customized kernel.

The SPECT data was reconstructed using OSEM[21] (seven iterations) and the micro-CT data using a Feldkamp[22] algorithm. The OSEM algorithm was a voxel-driven[23] implementation that incorporated the pinhole geometry, an interactive center-of-rotation correction, and the geometric response of a finite-sized pinhole using an inverse cone.[24] The micro-CT data was reconstructed using a previously described Feldkamp[22] conebeam reconstruction algorithm.[25]
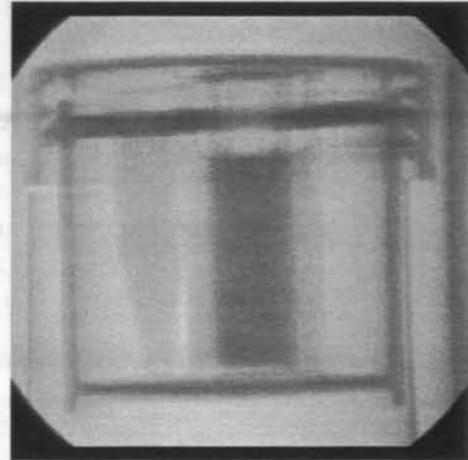
Using the SPECT reconstructed volume three horizontal and three vertical linescans near the center of each tube were averaged together to obtain full-width half-maximum (FWHM) diameter measurements in voxel units. The ratios between the known diameter of the tubes and the estimated diameters were used to compute the voxel dimension. This voxel dimension was multiplied by the number of voxels along one side of the reconstruction volume to determine its overall length. The pinhole-to-object distance was then determined by multiplying this length by the pinhole-to-detector distance divided by the detector diameter.

2.4. Results

Figure 1 shows a SPECT (left) and micro-CT (right) projection image of the test phantom obtained at the same angular position prior to reconstruction. One transaxial slice through the reconstructed SPECT volume is shown in figure 2(a). The FWHM diameter measurements indicated that the side of a voxel was ~ 0.67mm, with a resulting pinhole-to-object distance of 59.8mm. This voxel size was used in the registration algorithm. Figure 2(c) shows the same slice through the resulting micro-CT/SPECT registered volume, where the radioactivity in the SPECT volume is observable within the micro-CT image of the tubes.
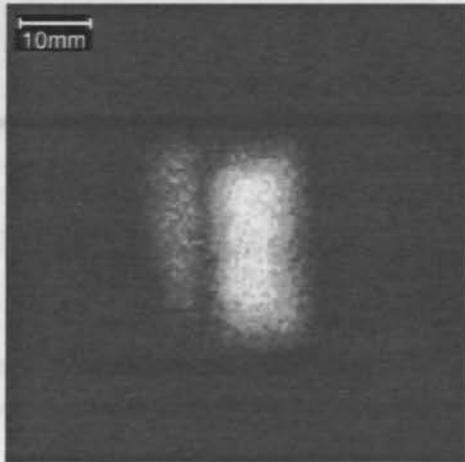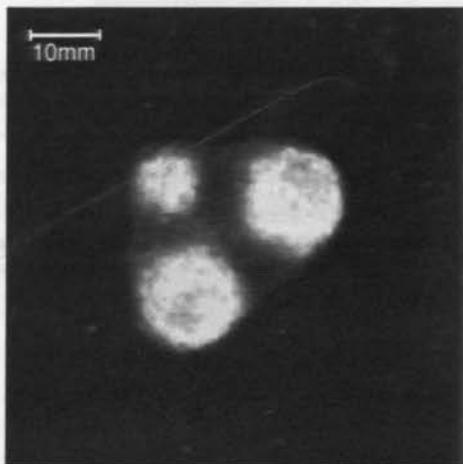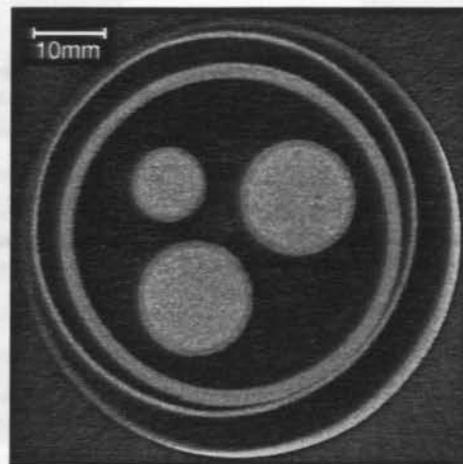

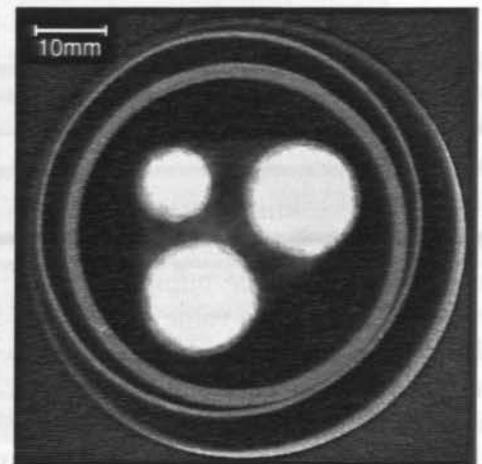(a) SPECT Phantom Projection   (b) Micro-CT Phantom Projection

Figure 1. (a) A SPECT projection image of the test phantom. Left side of image shows projection of small tube while right side shows superposition of the two larger tubes at this view. (b) Typical micro-CT projection image of the test phantom showing the small tube on the left side and the superposition of the two larger tubes on the right.

(a) SPECT Reconstruction   (b) Micro-CT Reconstruction   (c) Registered micro-CT/SPECT

Figure 2. (a) SPECT transaxial slice through the OS-EM reconstruction of the test phantom. (b) Micro-CT transaxial slice through the same phantom (c) Registered image of SPECT and micro-CT reconstructed transaxial slices.

3. PERFUSION STUDY

3.1. Preparation Methods

Seven Spraque-Dawley rats were studied using SPECT/micro-CT. Three of the rats were anesthetized with 75mg/kg ketamine and 0.5mg/kg medetomidine hydrochloride.[26] A 15mm opening in the chest was made between two consecutive ribs on the left side of the thorax and the left pulmonary artery separated from the bronchus and occluded with 5-0 suture. The left lung was then reinflated and the chest closed. After the surgery was completed an injection of 1mg/kg atipamezole hydrochloride was administered to assist in recovery. The rat was allowed to recover for ~40 days prior to subsequent imaging studies.

3.2. Imaging Methods

Four control rats (350g ±75.5) and three rats (500g ±83.9) that received occlusion surgery 40 days prior were imaged. Each rat was anesthetized with a mixture of 1.8mg/kg acepromazine and 82mg/kg ketamine.[26] A retrograde left carotid artery catheter was inserted and 2.0mCi of Tc99m MAA (1.0ml volume) was injected followed by a 0.5ml saline flush. The catheter was removed, the wound closed and the Tc99m MAA allowed to distribute via the systemic circulation (~ 2 minutes). The rat was then placed in a plastic tube (diam=70mm) and its thorax positioned in front of the pinhole collimator attached to the gamma camera. The object-to-pinhole distance was set to the same distance as used in the phantom calibration study and 128 projection images were acquired at 20sec/view. Without relocation, the rat was imaged using micro-CT with 360 angular views with an acquisition time of 233ms/view.

Following IA imaging, the rat was allowed to recover for at least 10 Tc99m halflives prior to subsequent IV imaging. The rat was anesthetized as before and a femoral venous catheter was inserted through which 2.0mCi of Tc99m MAA (1ml volume) was injected. The catheter was removed, the wound closed, and the rat imaged using SPECT and micro-CT as described above.

3.3. Image Processing

The two image volumes were then registered and segmentation was performed to identify the right and left lung in the SPECT volume. Because both the SPECT and micro-CT image acquisitions were performed without moving the rat, image registration required only the geometric parameters of the imaging system. The SPECT voxel size was determined by the phantom study since the same pinhole-to-object distance was used in both studies. The micro-CT voxel size was computed using the known source-to-object and source-to-image intensifier distances. The alignment of the x- and y- axis was accomplished by correcting the SPECT and micro-CT projection images for the center-of-rotation prior to reconstruction. Positioning the center of the gamma camera pinhole at the same height as the x-ray focal spot resulted in alignment of both image volumes in the z-direction. Determination of respective voxel sizes and x-, y-, z- alignment resulted in a mapping of the SPECT volume onto the micro-CT volume.

The whole lung in the micro-CT volume was segmented using an interactive 3D seeded region growing algorithm[27] by choosing a seed-point within the lung and a grayscale window. The lower limit of the window was chosen to be the minimum grayscale value within the volume, while the upper limit was chosen to be the maximum grayscale value within a region of interest positioned over the lung tissue free of any visible vessels. Slices above and below the lung were eliminated to prevent the algorithm from growing into the airfilled trachea or into regions representing reconstruction artifacts at the top or bottom portions of the volume. Morphological closing was implemented using a 2D dilation to incorporate unsegmented areas within the lung (primarily blood-filled vessels) followed by erosion to restore the bounderies of the region. The structuring element for these operations was chosen to be a disc with diameter equal to that of the largest unsegmented vessel within the lung. Once the entire lung field was segmented, the left and right lungs were identified manually.

The right and left lungs in the SPECT volume were identified by mapping the segmented micro-CT volume onto the SPECT volume using the developed registration algorithm. Counts within the left lung of the IA image volume and the right lung of the IV image volume were summed. The number of counts in the left lung was compared to the counts in the right lung to determine the percentage of left ventricular output perfusing the left lung via the bronchial circulation.

3.4. Results

Figure 3 shows transaxial slices through the registered volumes obtained from a control rat (no left pulmonary artery occlusion). Figure 3(a) shows activity in both lungs as well as the rest of the thorax due to the systemic circulation after an IA injection. Figure 3(b) was obtained from the same rat and shows activity in the lungs via the pulmonary circulation after an IV injection.
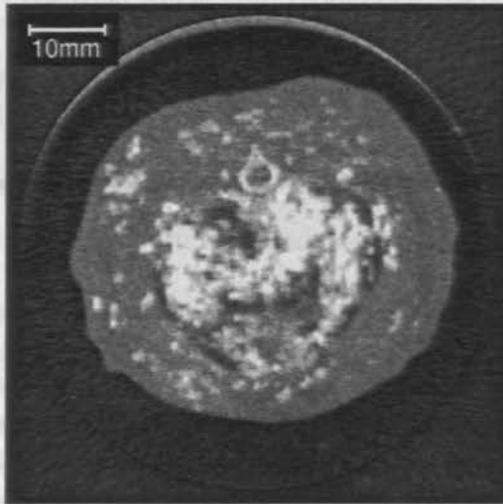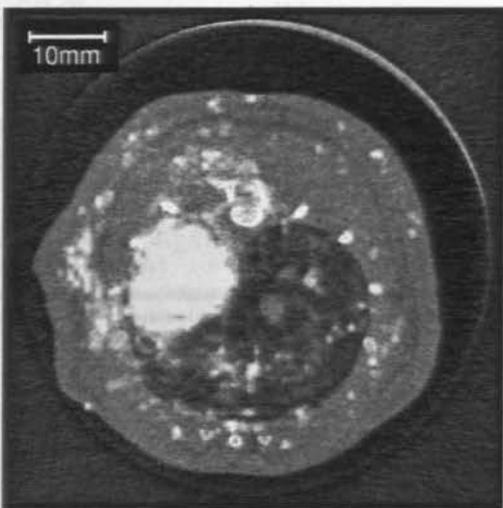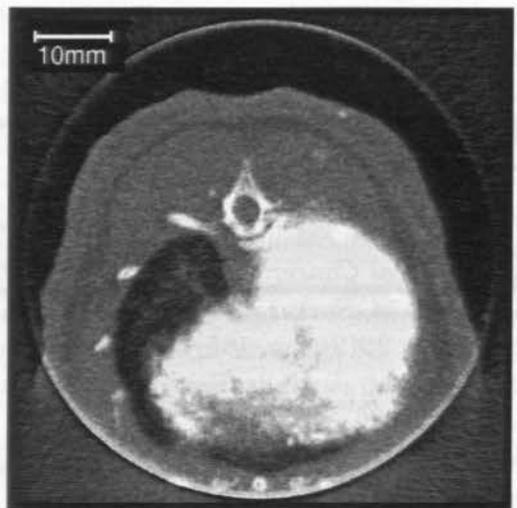

(a) Control IA Rat
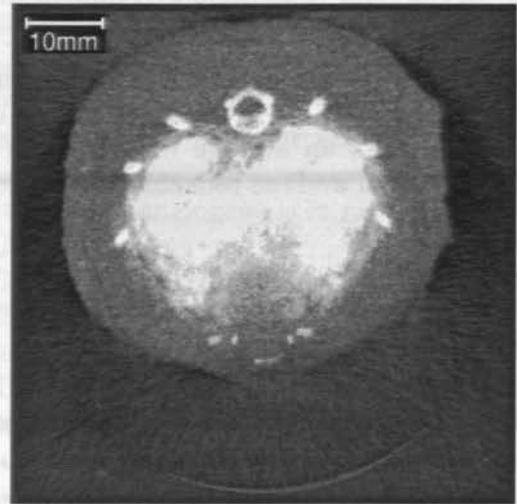
(b) Control IV Rat

Figure 3. (a) Transaxial slice through the registered volume of a control rat after IA injection. (b) Transaxial slice through the same rat after IV injection.

(a) Occluded IA Rat

(b) Occluded IV Rat

Figure 4. (a) Transaxial slice through the registered volume of a surgical occluded rat after an IA injection. (b) Transaxial slice through the same rat after IV injection.

Figure 4 shows transaxial images obtained from a rat 40 days following surgical occlusion of the left pulmonary artery. In figure 4(a) one observes a substantial increase in radioactivity in the left lung, as compared to the right lung or to the control rat image in figure 3(a), indicating an increase in perfusion derived from the bronchial circulation. Figure 4(b) shows that the IV injection of Tc99m MAA resulted in an accumulation of the radiotracer exclusively in the right (non-occluded) lung of the animal, where the left (occluded) lung is not perfused via the pulmonary circulation.

The ratio between the activity in the left lung after IA injection and activity in the whole lung after IV injection is a measure of the fraction of cardiac output that perfuses the left lung via the bronchial circulation. The control rats had an average bronchial circulation fraction of ~2.1% whereas the left pulmonary artery occluded rats had an average bronchial circulation fraction of 20.5% 40 days after the occlusion.

4. CONCLUSIONS

We have developed a methodology using micro-CT/SPECT imaging to quantify increase in bronchial circulation to the left lung after occlusion of the left pulmonary artery. The method appears to be successful in registering the lung regions within the SPECT and micro-CT image volumes. The quantification shows an overall increase in bronchial perfusion and future work will be aimed at analyzing the time course of this increase. This information can then be used to examine the mechanisms involved in the inhibition of angiogenesis in the bronchial circulation.

ACKNOWLEDGMENTS

REFERENCES

1. J. Folkman, "Role of angiogenesis in tumor growth and metastasis," *Seminar in Oncology* **29**, pp. 15–18, December 2002.
2. F. Hirsch, W. Franklin, A. Gazdar, and J. P.A. Bunn, "Early detection of lung cancer: Clinical perspectives of recent advances in biology and radiology," *Clin Cancer Res* **7**, pp. 5–22, January 2001.
3. R. Keith, Y. Miller, R. Gemmill, H. Drabkin, E. Dempsey, T. Kennedy, S. Prindiville, and W. Franklin, "Angiogenic squamous dysplasia in bronchi of individuals at high risk for lung cancer," *Clinical Cancer Research* **6**, pp. 1616–1625, May 2000.
4. D. Gross, I. Reibstein, L. Weiss, S. Slavin, I. Stein, M. Neeman, R. Abramovitch, and L. Benjamin, "The antiangiogenic agent linomide inhibits the growth rate of von hippel-lindau paraganglioma xenografts to mice," *Clinical Cancer Research* **5**, pp. 3669–3675, November 1999.
5. N. Lakhani, M. Sarkar, J.Venitz, and W. Figg, "2-methoxyestradiol, a promising anticancer agent," *Pharmacotherapy* **23**(2), pp. 165–172, 2003.
6. A. Guyton and J. Hall, *Textbook of Medical Physiology*, ch. 38, pp. 491–499. W.B. Saunders Company, nineth ed., 1996.
7. E. Weibel, "Early stages in the development of collateral circulation to the lung in the rat," *Circulation Research* **8**, pp. 353–376, March 1960.
8. F. Ellis, J. Grindlay, and J. Edwards, "The bronchial arteries. iii. structural changes after division of the rat's left pulmonary artery," *American Journal of Pathology* **28**, pp. 89–103, April 1952.
9. W. Shi, P. Cernacek, F. Hu, and R. Michel, "Endothelin reactivity and receptor profile of pulmonary vessels in postobstructive pulmonary vasculopathy," *American Journal of Pathology* **273**, pp. H2558–H2564, December 1997.
10. W. Mitzner, W. Lee, D. Georgakopoulos, and E. Wagner, "Angiogenesis in the mouse lung," *American Journal of Pathology* **157**, pp. 93–101, July 2000.

11. R. Michel and T. Hakim, "Increased resistance in postobstructive pulmonary vasculopathy: structure-function relationships.," *Journal of Applied Physiology* **71**, pp. 601–610, August 1991.

12. A. Padhani and M. Neeman, "Challenges for imaging angiogenesis," *The British Journal Radiology* **74**, pp. 886–890, October 2001.

13. M. Bajc, U. Bitzen, B. Olsson, V. P. de Sa, J. Palmer, and B. Jonson, "Lung ventilation/perfusion SPECT in the artificially embolized pig," *Journal of Nuclear Medicine* **43**, pp. 640–647, 2002.

14. E. M. F. Damen, S. H. Muller, L. J. Boersma, R. W. de Boer, and J. V. Lebesque, "Quantifying local lung perfusion and ventilation using correlated SPECT and CT data," *The Journal of Nuclear Medicine* **35**, pp. 784–792, 1994.

15. A. Pathak, K. Schmainda, B. Ward, J. Linderman, K. Rebro, and A. Greene, "MR-Derived cerebral blood volume maps: Issues regarding histological validation and assessment of tumor angiogenesis," *Magnetic Resonance in Medicine* **46**, pp. 735–747, 2001.

16. T. Purdie, E. Henderson, and T.-Y. Lee, "Functional CT imaging of angiogenesis in rabbit VX2 soft-tissue tumour," *Physics in Medicine and Biolog* **46**, pp. 3161–3175, 2001.

17. C. Wietholt, R. Molthen, R. Johnson, C. Dawson, and A. Clough, "SPECT imaging of pulmonary blood flow in a rat," in *Proceedings of the SPIE Medical Imaging 2003: Physiology and Function: Methods, Systems, and Applications*, A. Clough and A. Amini, eds., **5031**, pp. 252–261, May 2003.

18. R. Johnson, H. Hu, S. Haworth, P. Cho, C. Dawson, and J. Linehan, "Feldkamp and circle-and-line cone-beam reconstruction for 3D micro-CT of vascular networks," *Physics in Medicine and Biology* **43**, pp. 929–940, 1998.

19. R. Molthen, S. Haworth, D. Roerig, C. Hanger, R. Johnson, and C. A. Dawson, "Cone-beam x-ray micro-computed tomography with concurrent dynamic planar angiographic imaging and physiological measurement," in *High Resolution Imaging in Small Animals: Instrumentation, Applications and Animal Handling, Proc. HiRes*, pp. 253–255, 2001.

20. R. Molthen, C. Wietholt, S. H. S., and C. Dawson, "Estimation of pulmonary arterial volume changes in the normal and hypertensive fawn-hooded rat from 3D Micro-CT data," in *Proc. of SPIE Medical Imaging 2002 Physiology and Function from Multidimensional Images*, C. C.-T. Clough A., ed., **4683**, pp. 266–275, SPIE, Feb. 2002.

21. H. Hudson and R. Larkin, "Accelerated image reconstruction using ordered subsets of projection data," *IEEE Transactions on Medical Imaging* **13**, pp. 601–609, December 1994.

22. L. Feldkamp, L. Davis, and J. Kress, "Practical cone-beam algorithm," *Journal of Optical Society of America A* **1**, pp. 612–619, June 1984.

23. N. Schramm, *Entwicklung eines hochaufloesenden Einzelphotonen-Tomographen fuer kleine Objekte*. PhD thesis, Universitaet Goéttingen, 2001.

24. G. Zeng, G. Gullberg, B. Tsui, and J. Terry, "Three-dimensional iterative reconstruction algorithms with attenuation and geometric point response correction," *IEEE Transactions on Nuclear Science* **38**, pp. 693–702, April 1991.

25. R. Johnson, R. Molthen, K. Karau, C. Hanger, S. Haworth, C. Dawson, and J. Linehan, "Analysis of 3D pulmonary microangiograms," in *Computer-aided Diagnosis in Medical Imaging*, K. Doi, H. MacMahon, M. Giger, and K. Hoffmann, eds., *Excerpta Medica International Congress Series* **1182**, pp. 369–376, (Amsterdam), 1999.

26. P. Sharp and M. LaRegina, *The Laboratory Rat*, ch. 4, pp. 101–113. The Laboratory Animal Pocket References Series, CRC Press LLC, 1998.

27. M. Fiebich, C. Wietholt, B. Renger, S. Armato, K. Hoffmann, D. Wormanns, and S. Diederich, "Automatic detection of pulmonary nodules in low-dose screening thoracic CT examinations," in *Proc. of SPIE Medical Imaging 1999: Image Processing*, H. K.M., ed., **3661**, pp. 1434–1439, SPIE, May 1999.